A METHOD ON MODELING AND VISUALIZATION OF 3D OBJECT

Wang Zhi [a], LI Qingquan [b,*], LI Yuguang [a]

[a] Research Center of Spatial Information and Network Communication, Wuhan University,
129 Luoyu Road, Wuhan, China, 430079 - wangzhimail@21cn.com, wd_liyuguang@yahoo.com.cn
[b] State Key Laboratory of Information Engineering in Surveying ,Mapping and Remote Sensing , Wuhan University,
129 Luoyu Road, Wuhan, China, 430079 - qqli@whu.edu.cn

KEY WORDS: Three-dimensional (3D) object modelling, 3D Visualization, TIN, Multi-resolution, Edge collapses

ABSTRACT:

Three-dimensional (3D) digital modeling of object through optical scanners has been demonstrated in recent years with results of exceptional interest. However, the routine application of 3D modeling and visualization still requires the systematic investigation of a number of technical problems. In this paper, a 3D modeling and visualization techniques is proposed. Using a 3D shape acquisition system we introduced and this modeling method, users can reconstruct accurate models in appropriate date amount. In this paper, triangulated irregular network (TIN) model is utilized and taken as basis in modelling of 3D object, making use of the polygonal structure and vertex coordinates for the visualization of 3D models. In this paper, TIN mesh simplification algorithm, using unified stencil and based on multi-resolution adjustment, is also proposed to utilize data amount adjustable 3D modeling and reduce the difference between low and high resolution models so that model resolution and transmitted data amount can be regulated according to visitor's requirement. Finally, some experimental results are illustrated and further analyses are discussed.

1. INTRODUCTION

Three-dimensional (3D) modeling of object shapes is commonly utilized in several applications such as computer graphics, computer aided design, computer games, object recognition and the area of cultural heritage. 3D scanning in the area of cultural heritage is to produce content that can be used for the education of students and for informing the general public.

One way of obtaining 3D model polygonal of an object is to utilize 3D scanners. In this paper, we will introduce a 3D acquisition system in a high accuracy way (MSE is lower than 0.1mm). There are also multiple 3D modeling techniques (Chen, 2002; Godin, 2002) and each has its own advantages and drawbacks depending on the application area. However, the polygonal modeling with triangular facets has become the de facto standard for representation of 3D shapes on computers. Polygonal models are commonly preferred mainly because of their simplicity in representing complex shapes and ease of handling. A polygonal model consists of three kinds of mesh elements, namely vertices, edges and faces (usually triangles). These elements are used to describe the mesh geometry and mesh connectivity. A common approach is to keep a list of vertex coordinates to define the geometry, and a second list of polygon connectivity information (for face-based structures) or edge connectivity information (for edge-based structures).

However, scanned 3D object models can consist of millions of vertices, and although a higher sampling rate means improved shape resolution, the high data amount can be impractical for some applications requiring real-time rendering, manipulation, storage or transmission. Simplification algorithms are essential for reducing the data amount if the original 3D model is sampled at high resolution and a lower resolution is sufficient for the application. As this is commonly the case if 3D models are acquired by laser scanners, a lot of research has been carried out in the field of mesh simplification.

Various mesh simplification algorithms have been proposed in the literature. Vertex clustering by merging cells to cells or clusters and representing each cell by one vertex (Rossignac et al, 1993) has been proposed. Face clustering (Kalvin A. D. et al, 1996) has been proposed, by merging coplanar faces to superfaces, with the utilization of error metrics to keep the topology, however it was difficult to triangulate the patches and there was a possibility of creating holes in the model. Progressive meshes (PM) have been a well-known method for mesh simplification based on the edge collapses or edge contraction operation, where a single vertex was removed at each time (Hoppe, 1996; Hoppe et al, 1993). While the method is time-consuming and hence not appropriate for real-time mesh simplification applications, it provides simple and effective means for offline stabilization. A multiphase approach consisting of an initial out-of-core uniform vertex clustering, followed by an in-core iterative edge contraction (Garland et al, 2002) has been proposed. Zorin D. et al described a multi-resolution representation for meshes based on subdivision (Zorin et al, 1997), which was a natural extension of the existing patch-based surface representations. Cignoni et al presented a data structure called Octree-based External Memory Mesh (OEMM) (Cignoni et al, 2003). It supports external memory management of complex meshes, loading dynamically in main memory only the selected sections and preserving data consistency during local updates. Recently, Bisheng Yang, Qingquan Li and Wenzhong Shi proposed a new

The work described in this paper was fully supported by the National Natural Science Foundation of China (Project No.: 40301040)

approach (Bisheng et al, 2005), which extended the iterative edge collapses and vertex splits algorithm, to dynamically generate multi-resolution TIN models. Moreover, they defined a set of rules to improve the validity judgment of vertex splits and edge collapses.

The paper is organized as follows: The first part of the paper introduces significant previous works of 3D modeling and visualization. In section 2, we take a closer look on a highly accurate acquisition system which we used to get the 3D data of object. We describe a profile sampling algorithm in this section. Modelling approach and mesh generation method are also described in this section. In section 3, we propose a new TIN mesh simplification algorithm using unified stencil based multi-resolution adjustment. In section 4, experimental results are presented. Models and visualisation results are given in this part, followed by conclusions and outlook on future work.

2. 3D SHAPE ACQUISITION SYSTEM

2.1 System Configuration

The acquisition system consists of the following parts (Figure 1): a turntable, a motor driver, a monochrome camera (1300×1030 pixels) employing a lens with 16mm focal length and a linear structured light projector mounted in fixed position on a rigid structure, and software.

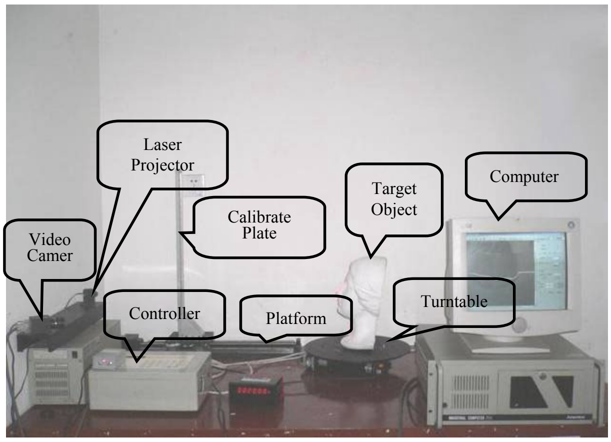

Figure 1. Hardware setup of 3D shape measurement system.

As shown in the schematic diagram (Figure 2), the laser projector projects a beam of linear structured light at the 3D object while rotating the object on a turntable. The projected structured light is captured by the high resolution camera. The shape of line structured light in each image (Figure 3) corresponds to a profile of objects of real-world. With our proposed method, 3D points in these profiles can be acquired by our 3D acquisition system and converted to the object coordinate system by using rotation angle. The method for acquiring the 3D shape of an object is based on active triangulation (Szeliski, 1993). The accurate 3D model of an object (MSE<0.1mm) can be reconstructed by integrating all the data.

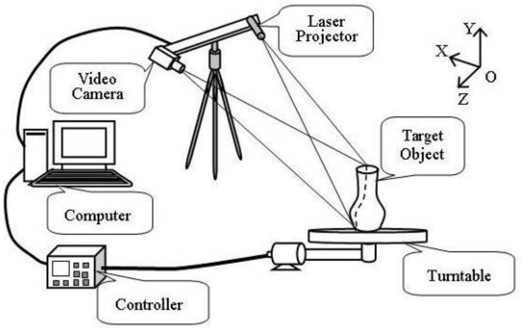

Figure 2. Connections of 3D shape acquisition system.

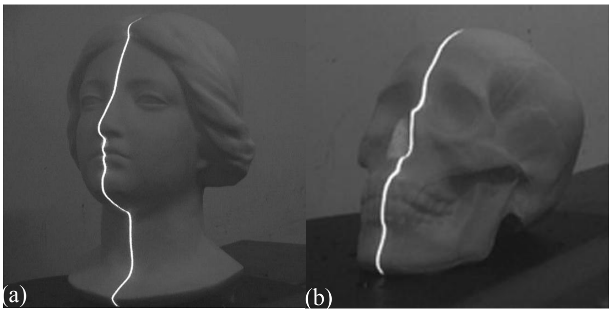

Figure 3. 2D images of objects.

2.2 Modeling Approach

The transformation relationship between the point P_c (x_c, y_c) in the camera coordinate system and the homologous point P_W $(x_W, y_W, 0)$ in the world coordinate system can be expressed with a cubic polynomial. After calibration, we can convert 3D points' coordinates to coordinates in a cylinder polar coordinate using equation 1:

$$\begin{cases} \rho_i = | x_w - x_{axis} | = | x_w - (a + by_w) | \\ \theta_t = \omega_t \\ z = y_w \end{cases} \tag{1}$$

Where i = index of 3D point $(0 < i < n)$

x_{axis} = x coordinates of rotation axis

ω_t = rotation angle $(0^\circ \le \omega_t < 360^\circ)$

$P(\rho_i, \theta_t, z_i)$ = object coordinates in cylinder coordinate system

Then we convert points' coordinates in the cylinder polar coordinate system to points' coordinates in the world coordinate system (see Figure 4) for the modelling and visualization of 3D object by using rotation and equation 2:

$$\begin{cases} X_w = \rho_i \times \cos\theta_t \\ Y_w = \rho_i \times \sin\theta_t \\ Z_w = z_i \end{cases} \tag{2}$$

Where $P(X_w, Y_w, Z_w)$ = object coordinates in world coordinate system

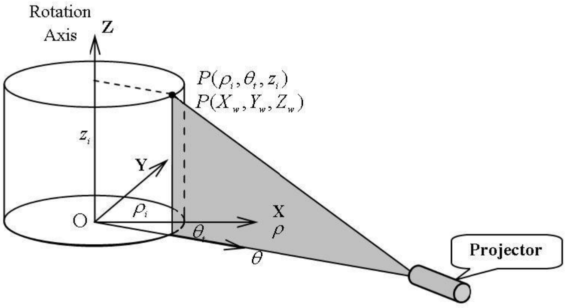

Figure 4. Coordinate system.

2.3 The proposed profile sampling algorithm

Figure 3 shows the shape of line structured light which corresponds to a profile of objects. If higher sampling in the profiles and converting it to the object coordinate system, we will get a high resolution 3D vertices model with a large volume of data. Sometimes, lower resolution is sufficient and we can equidistantly lower sampling to get a considerable resolution model with a appropriate volume of data.

In this paper, we proposed a profile sampling algorithm which sampling with a sample filter and hold the vertices which have most geometric contributions. The profile sampling algorithm is not carried out in a random fashion for vertices that have most geometric contribution are kept. The sampling algorithm is carry out in each profile of 3D objects. The initial step of the algorithm is choice length of filter. The length of filter can be 5, 10, … , 15, 20, … . We calculated MSE (Mean Square Errors) of the points' coordinates in profile within the range of filter using Equation 3:

$$\sigma=\sqrt{\frac{\sum_{i=0}^{L-1}(\rho_i-\rho_{aver})^2}{n-1}} \tag{3}$$

Where, L is the range of sample filter and i $(0 \le i < L)$ is the index of 3D points in profile. $P(\rho_i, \theta_t, z_i)$ is a 3D point in cylinder polar coordinate system (Figure 3), ρ_i is the radius of point and Z_i is the height which index is i $(0 \le i < L)$, and θ_t is the rotation angle. ρ_{aver} is average of the points' radius in range of sample filter (Equation 4).

$$\rho_{aver}=(\sum_{i=0}^{L-1}\rho_i)/L-1 \tag{4}$$

In a given range of sample filter, the difference between ρ_{aver} and ρ_i of each point is evaluated. The MSE of the filter is a direct measure and indicate of the 3D points' geometric contribution in the range of sample filter. If difference between ρ_{aver} and each vertices' ρ_i is not larger than treble MSE (3σ), it states that the corresponding all the points in this filter has little geometric contribution, which can be deleted from the profile and replaced with one point $P_{aver}(\rho_{aver}, \theta_t, z_{aver})$, where ρ_{aver} is average radius of points'. We can do that safely and get a considerable resolution model after sampling processing. Correspondingly, if any of the difference between ρ_{aver} and ρ_i is larger than treble MSE, it means the radius of points are relatively great discrepant in this range of sample filter. It also means we should add all the points in this sample filter to vertices model.

During the procedure, vertices tally with our qualification are consecutively sampled and added to the vertices model. We keep moving the sample filter along every profile and sampling procedure is repeated. We get a considerable resolution vertices model until all the profiles are processed. The main structure of the algorithm is given below (Figure 5).

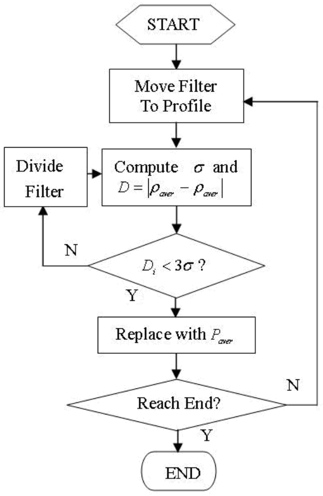

Figure 5. Pipeline of profile sampling algorithm.

2.4 Mesh generation

The 3D vertices can be improved by removing scan points that remain isolated, and by filling small holes surrounded by geometry using linear interpolation between neighboring depth pixels. Triangulated irregular network (TIN) is a popular model for representing surface models in geographic information systems (GIS), computer graphics, and virtual reality (VR) because it has a simple data structure and can easily be rendered using common graphics hardware. The amount of polygons and vertices of a model is proportional to the resolution as well as data quantity. In other words the resolution and data increases with the number of polygons. To represent the details of a model, a high resolution TIN model (with dense triangles) should be used in our proposed modeling approach.

We use a mesh of triangles to represent the 3D data at all stages of our integration method. Each sample point in the 3D vertices is a potential vertex in the triangle mesh. We use method (Früh et al, 2002) proposed by Früh C. and Zakhor A. to build a mesh. We take special care to avoid inadvertently joining portions of the surface together that are separated by depth discontinuities. We find the shorter of the two diagonals between the points and use this as first criteria to identify the two triplets of points that may become triangles. Each of these point triples is made into a triangle if the edge lengths fall below a distance threshold. Let

s_{max} be the maximum distance between adjacent range points when we flatten the range image, that is, when we don't include the depth information. We take the distance threshold be a small multiple of this sampling distance, typically $4s_{max}$ (Greg et al, 1994). Neighbors are also connected if their depth difference does exceed the threshold $4s_{max}$ and the local angle between neighboring points is smaller than threshold angle φ_{max} . The second criteria is intended to connect neighboring points that are on a line, even if their depth difference exceeds $4s_{max}$. The resulting quadrilateral mesh is split into triangles. So neighbor 3D vertices are connected, if

$$\left|s_{n+\Delta n,v+\Delta v} - s_{n,v}\right| < 4s_{max} \quad \text{or if} \quad \cos\varphi > \cos\varphi_{max} \tag{5}$$

$$\text{Where } \cos\varphi = \frac{(\vec{P}_{n-\Delta n,v-\Delta v} - \vec{P}_{n,v})\cdot(\vec{P}_{n,v} - \vec{P}_{n+\Delta n,v+\Delta v})}{\left|\vec{P}_{n-\Delta n,v-\Delta v} - \vec{P}_{n,v}\right|\cdot\left|\vec{P}_{n,v} - \vec{P}_{n+\Delta n,v+\Delta v}\right|} \tag{6}$$

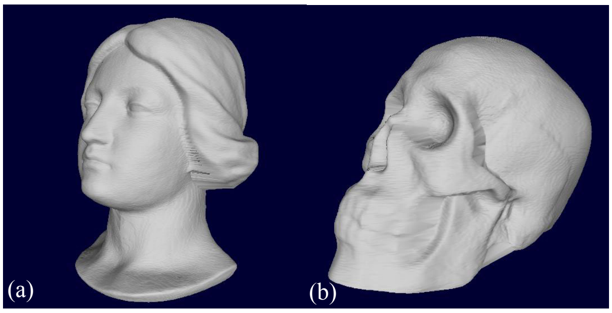

Figure 6. 3D models of objects.

Figure 6 shows the 3D models of objects (Figure 3) reconstructed by the integration method we proposed in this paper.

3. THE PROPOSED SIMPLIFICATION APPROACH

In this paper, we represented a TIN simplification algorithm which accomplishes edge collapses so that 3D models with varying level of detail are obtained. The support for refinement enables that users can initially download the low resolution model to have a first view of the object, without having to download the bulk data for an initial look. After viewing the low resolution model, the user can refine the model if desired.

3.1 QEM-based Mesh Simplification

The QEM method (Garland et al, 1997) was originally defined for simplification of triangle meshes. Each vertex of the original mesh sits at the intersection of the planes of its adjacent triangles, which amounts to a summed distance of zero to all these planes. The squared distance of a vertex with position to one such plane $P = [a \quad b \quad c \quad d]$ is elegantly expressed in the quadratic form: $d(p) = p^T Qp$, where

$$Q = \begin{bmatrix} a^2 & ab & ac & ad \\ ab & b^2 & bc & bd \\ ac & bc & c^2 & dc \\ ad & bd & cd & d^2 \end{bmatrix} \tag{7}$$

Summing up a set of quadrics Q_i results in a new quadric $\tilde{Q} = \sum_i Q_i$, which can be used to measure the sum of squared distances to the set of planes defined by the Q_i .The QEM simplification algorithm is initialized by assigning to each mesh vertex the sum of quadrics representing the planes of its adjacent triangles. For evaluating a prospective collapse of edge with end vertices u and v , the quadrics Q_u and Q_v are summed up: $Q_{uv} = Q_u + Q_v$. The position of the collapsed vertex p_{uv} that minimizes the squared distance to the set of planes defined by Q_{uv} is then calculated by solving the linear equation $\nabla d(p_{uv}) = 0$. The value of $d(p_{uv})$ represents the estimated surface approximation error, and is used to rank this collapse operation. In the main loop of the algorithm, when the current "best collapse" is read from the queue and carried out, the new vertex position is set to the optimal position, and the potential collapses along the changed edges are reevaluated. Due to the simple and fast evaluation of the error metric, QEM simplification is very fast, and produces generally pleasing results.

3.2 Pyramid Scheme

The butterfly scheme (Dyn et al, 1990) is developed by Dyn and Levin in 1990. This scheme is interpolating, local, and simple to implement, but only leads to C^1 surfaces in the regular setting. Zorin, Schröder, and Swelden developed it to handle the extraordinary vertices, which the existing scheme ignored. In this paper, we will give a more direct route, pyramid interpolating scheme, using an unified stencil by interpolation without requiring the solution of a global linear. We developed it to handle all of the vertices pairs to be collapsed, including the extraordinary vertices. For using an unified stencil and interpolation parameters are determined by number of conjunction vertices and the way they connect, the pyramid interpolating scheme is easy to program. As shown in Figure 7, $\tilde{v}$ denotes the new vertex that is being added and the labeled vertices are the vertices used to interpolate the new coordinates for that vertex in three-dimensional space. We then assign rules on how to compute the interpolated value.

As shown in Figure 7, (v_1, v_2) is the vertex pair to collapse. v_3 and v_4 are two additional vertices to the up and down of the collapsed edge. $v_5, v_6, \ldots, v_9, v_{10}$ vertices are in conjunction with vertices v_1 and v_2 . $\tilde{v}$ is the new interpolating point.

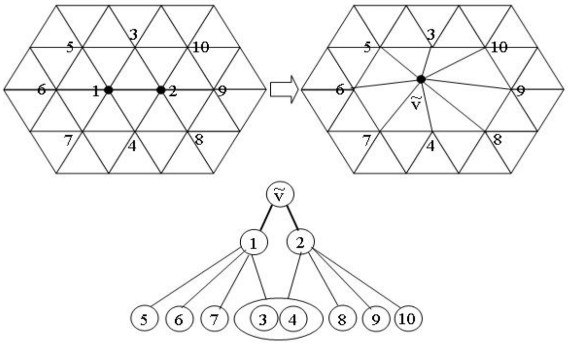

Figure 7. Pyramid bracketing algorithm.

In order to perform the contraction $(v_1, v_2) \rightarrow \tilde{v}$, we must also choose the position of v. A simple scheme would be to select either v_1, v_2 or $(v_1 + v_2)/2$ depending on which one of these produces the lowest approximation error value of $\tilde{v}$. In the pyramid interpolating algorithm we proposed, we use Equation 8 to compute the position of $\tilde{v}$:

$$\tilde{V} = \frac{1}{2}(V_1 + V_2) + \frac{1}{4 \times m}\sum_1^m V_i - \frac{1}{4 \times n}\sum_1^n V_j \qquad (8)$$

Where, (v_1, v_2) is the vertex pair to collapse, and v_i is additional vertex in conjunction with v_1 and v_2. v_j is vertex in conjunction with v_1 or v_2. $\tilde{v}$ is the new interpolating vertex. For the mesh shown in Figure 7, we use Equation 9 to compute position of $\tilde{v}$.

$$\tilde{V} = \frac{1}{2}(V_1 + V_2) + \frac{1}{4 \times 2}(V_3 + V_4) - \frac{1}{24}(V_5 + V_6 + V_7 + V_8 + V_9 + V_{10}) \qquad (9)$$

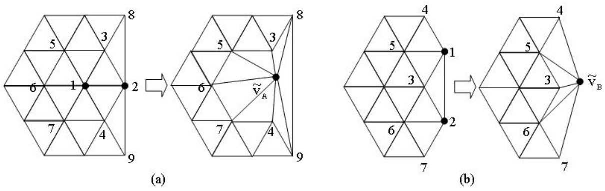

Figure 8. Boundary edge collapses.

As shown in Figure 8, for the case where an edge contains a vertex of valence 6 and another edge in boundary contains extraordinary vertex which is not of valence 6, the unified vertex stencil is used in our interpolating algorithm on the extraordinary vertices with the following Equation 10 and Equation 11 respectively:

$$\tilde{V}_A = \frac{1}{2}(V_1 + V_2) + \frac{1}{4 \times 2}(V_3 + V_4) - \frac{1}{20}(V_5 + V_6 + V_7 + V_8 + V_9) \qquad (10)$$

$$\tilde{V}_B = \frac{1}{2}(V_1 + V_2) + \frac{1}{4}(V_3) - \frac{1}{16}(V_4 + V_5 + V_6 + V_7) \qquad (11)$$

3.3 TIN Simplification Algorithm Summary

Our TIN simplification algorithm is built around error quadrics and pair contractions. The current implementation represents models using an adjacency graph structure: vertices, edges, and faces are all explicitly represented and linked together. To track the set of valid pairs, each vertex maintains a list of the pairs of which it is a member. The algorithm itself can be quickly summarized as follows:

1. Compute the Q matrices for all the initial vertices.
2. Select all valid pairs.
3. Compute the optimal contraction target $\tilde{v}$ for each valid pair (v_1, v_2). The error $d(p_{uv})$ of this target vertex becomes the cost of contracting that pair.
4. Place all the pairs in a heap keyed on cost with the minimum cost pair at the top.
5. Iteratively remove the pair (v_1, v_2) of least cost from the heap, store the information of pair (v_1, v_2) in enhancement layer for model refinement, contract this pair, compute the new position of $\tilde{v}$, and update the costs of all valid pairs involving $\tilde{v}$.

4. EXPERIMENTAL RESULTS

To evaluate the efficiency of our modelling and simplification method, we measure objects and construct 3D models of them. We will now present the system's reconstruction and simplification results.

Figure 9 and Table 1 show the results of profile sampling and demonstrates the amount of VRML model data involved during the process for the "Skull" and "Portrait" models. Profile sampling results are listed in Table 1. Figure 10 and Figure 11 show the results of TIN simplification approach we proposed. As shown in Table 2, at the lower resolution (model b) the data amount required to represent the model is 2,191 Kbytes. The enhancement layer comprising the point and polygons information required to build the model with one high resolution level (model a) takes 1,028 Kbytes, so that a total of 5,013 Kbytes of data is required if the model is refined from the lower resolution (compare to the necessary 3,985 Kbytes to represent "model a" unaided). In this way, the total amount of data required to construct the highest resolution model (model a) from the lowest resolution model (model d) by refinement is 7,813 Kbytes, almost twice as much compared to the 3,985 Kbytes required to represent the highest resolution model by itself. Though the model in highest compress rate becomes a little smoother and the computational costs will increase by using our TIN simplification algorithm, it is still important to accept for having a multi-resolution scheme. With multi-resolution scheme, it is also possible to give the user two choices, to download the lowest resolution model or the highest resolution model. However in latter case the user will have to wait until the entire data of the highest resolution model is downloaded before it can be viewed. In order to introduce a lighting effect, so that every facet is rendered according to a light source located in the 3D space, the normal of each triangle is calculated using the Newell method (McReynolds et al, 1998) to provide brightness values that vary according to the surface normal. In the experiment, we use Intel Pentium 4 CPU-2.80 GHz processor with 256 DDR RAM running on a Windows XP OS.

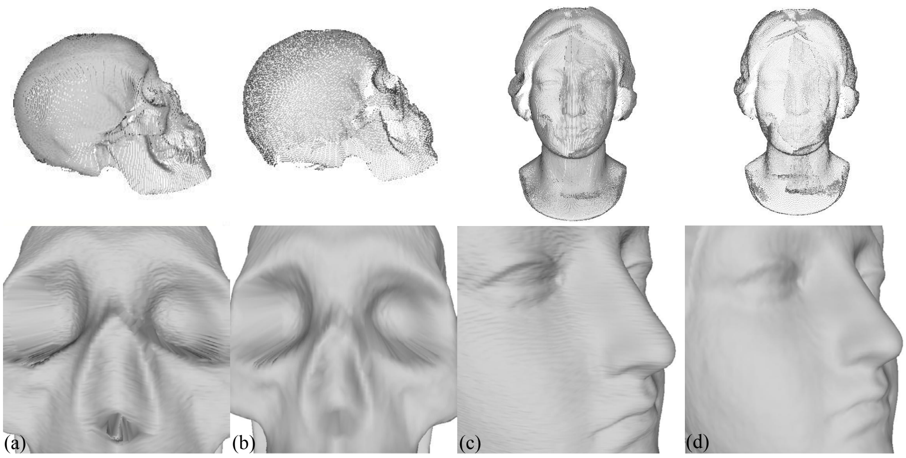

Figure 9. 3D visualization results of model after profile sampling:
(a) Triangle number=139,931, vertex number=282,234;
(b) Range of sample filter=5, triangle number=28,634, vertex number=57,168;
(c) Triangle number=249,412, vertex number=497,342;
(d) Range of sample filter=5, triangle number=50,181, vertex number=100,182.

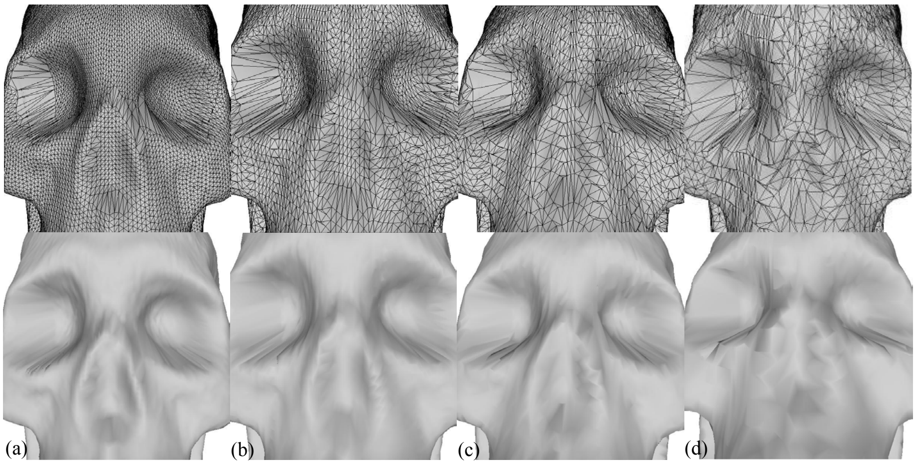

Figure 10. 3D visualization results of multi-resolution skull TIN model:
(a) Triangle number=28,634, vertex number=57,168; (b) Triangle number=16,000, vertex number=31,951;
(c) Triangle number=12,000, vertex number=22,729; (d) Triangle number=8,000, vertex number=15,964.

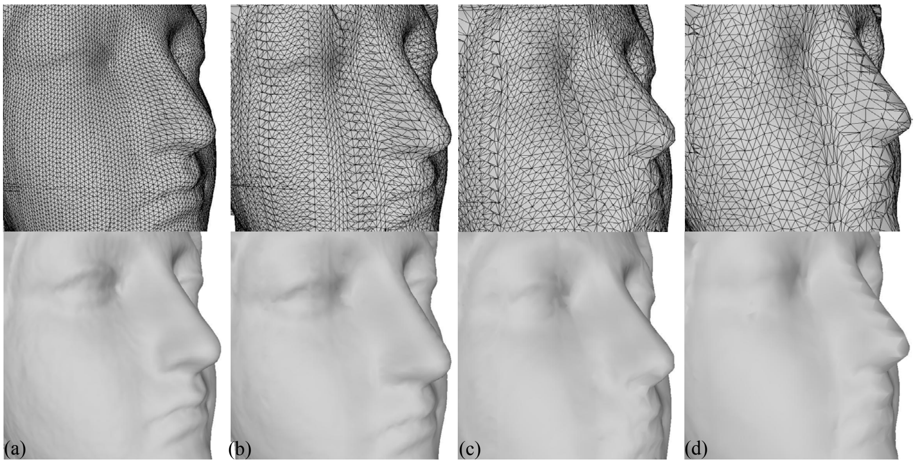

Figure 11. 3D visualization results of multi-resolution portrait TIN model:
(a) Triangle number=50,181, vertex number=100,182; (b) Triangle number=25,000, vertex number=55,796;
(c) Triangle number=20,000, vertex number=39,934; (d) Triangle number=12,000, vertex number=28,526.

	Range of filter	Vertices	Polygons	Data (KB)
Skull	—	139,931	282,234	11,517
	5	28,634	57,168	2,230
Portrait	—	249,412	497,342	21,423
	5	50,181	100,182	3,985

Table 1. Results of profile sampling (Figure 9).

	Level	Vertex numbers	Polygon numbers	Compress rate (%)	Data (KB)
Skull	a	28,634	57,168	—	2,230
	b	16,000	31,951	44	1,218
	c	12,000	22,729	58	848
	d	8,000	15,964	72	587
Portrait	a	50,181	100,182	—	3,985
	b	25,000	55,796	50	2,191
	c	20,000	39,934	60	1,550
	d	12,000	28,526	76	1,089

Table 2. Comparison between different levels of detail (Figure 10 and Figure 11).

5. CONCLUSION AND OUTLOOK

We presented a method of modeling and visualization that is able to recover objects with an arbitrary topology and adapts its resolution according to object geometry and visitor's requirement. A TIN simplification algorithm using unified stencil is also proposed. Contrast to butterfly interpolation scheme, the pyramid interpolating scheme use unified stencil for interpolation and interpolation parameters are determined by number of conjunction vertices and the way they are connected. With this TIN simplification algorithm high resolution models are iteratively simplified by edge collapses, to obtain a multi-resolution representation scheme with various levels of detail as well as varying data amount. The structure information dropped during each edge collapses step is saved in an enhancement layer that is used to reconstruct high resolution models from lower resolution ones through refining. Experimental results show that our model provides enhanced segmentation quality. Further works will focus on the method that can significantly reduce computational and memory costs.

REFERENCE

[1] Chen F., Brown G. M., and Song M., 2002. Overview of Three-Dimensional Shape Measurement Using Optical Methods, *Optical Engineering*, vol. 39, no. 1, pp. 10-22.

[2] Godin G., Beraldin J. A., Taylor J., Cournoyer L., Rioux M., El-Hakim S., Baribeau R., Blais F., Boulanger P., Picard M. and Domey J., 2002. Active optical 3D imaging for heritage applications, in *Proc. IEEE Computer Graphics & Applications. Special Issue on Computer Graphics in Art History & Archaeology*, vol. 22, pp. 24-36.

[3] Rossignac J. and Borrel P., 1993. Multi-resolution 3D approximations for rendering, Modeling in Computer Graphics, pp. 455-465.

[4] Kalvin A. D. and Taylor R. H., 1996. Superfaces: Polygonal mesh simplification with bounded error. IEEE Computer Graphics & Applications, vol. 16(3), pp. 64-77.

[5] Hoppe H., 1996. Progressive meshes, Proceedings of SIGGRAPH 96, pp. 99-108.

[6] Hoppe H., DeRose T., Duchamp T., McDonald J. and Stuetzle W., 1993. Mesh Optimization, Proceedings of SIGGRAPH 93, pp. 19-20.

[7] Garland M. and Eric S., 2002. A Multiphase Approach to Efficient Surface Simplification, Proceedings of IEEE VIS 2002, pp. 117-124.

[8] Zorin D., Sweldens W. and Schröder P., 1997. Interactive Multiresolution Mesh Editing, in the Proceedings of ACM SIGGRAPH '97, pp. 259-268.

[9] Cignoni P., Montani, C., Rocchini C. and Scopigno R., 2003. External Memory Management and Simplification of Huge Meshes, IEEE Trans. on Visualization and Computer Graphics.

[10] Bisheng Yang, Qingquan Li and Wenzhong Shi, 2005. Constructing multi-resolution triangulated irregular networkmodel for visualization. Computers & Geosciences vol. 31, pp.77-86.

[11] Szeliski R., 1993. Rapid Octree Construction from Image Sequences. *CVGIP: Image Understanding*, vol. 58(1), pp. 23-32.

[12] Früh C. and Zakhor A., 2002. Data processing algorithms for generating textured 3D building facade meshes from laser scans and camera images, 3D Processing, Visualization and Transmission 2002, Padua, Italy, pp. 834 -847.

[13] Greg T. and Marc L., 1994. Zippered Polygon Meshes from Range Images, Proc. SIGGRAPH '94, In *Computer Graphics* Proceedings, Annual Conference Series, pp. 311-318.

[14] Garland M. and Paul S., 1997. Surface simplification using quadric error metrics. In *Computer Graphics (Proc. SIGGRAPH 97)*, pp. 209-216.

[15] Dyn N., Levin D. and Gregory J. A., 1990. A butterfly subdivision scheme for surface interpolation with tension control. *ACM Transactions on Graphics*, vol. 9(2), pp.160-169.

[16] McReynolds T. and Blythe D., 1998. Advanced Graphics Programming Techniques Using OpenGL, Silicon Graphics, Siggraph'98 Course Notes, ACMSIGGRAPH.